Available online at www.sciencedirect.com
ScienceDirect
Physica D 237 (2008) 50–65
PHYSICA D
www.elsevier.com/locate/physd

Asymptotics for kink propagation in the discrete Sine-Gordon equation

L.A. Cisneros[a,*], A.A. Minzoni[b]

[a] *Graduate Program in Mathematical Sciences, Facultad de Ciencias, Universidad Nacional Autónoma de México, Apdo. 20-726, 01000 México, D. F., Mexico*
[b] *FENOMEC, Department of Mathematics and Mechanics, IIMAS, Universidad Nacional Autónoma de México, Apdo. 20-726, 01000 México, D. F., Mexico*

Received 29 November 2006; received in revised form 18 July 2007; accepted 7 August 2007
Available online 21 August 2007

Communicated by Y. Nishiura

Abstract

The evolution of a propagating kink in a Sine-Gordon lattice is studied asymptotically using an averaged Lagrangian formulation appropriately coupled to the effect of the radiation. We find that unlike the continuum case the interaction with the Goldstone mode is important to explain the acceleration of the kink as it hops along the lattice. We develop a discrete WKB type solution to study the interaction of the kink and the radiation. In particular using this solution we show how to calculate the effect of the Peyrard and Kruskal resonant radiation in the energy loss of the kink. We obtain a set of modulation equation which explains qualitatively the evolution of the kink with remarkable quantitative agreement.

Keywords: Kink; Peierls–Nabarro potential; Radiation damping; Internal modes; Modulation averaged Lagrangian

1. Introduction

Since 1938 when Frenkel and Kontorova [1] introduced their model, which describes a chain of harmonically coupled particles subjected to an external periodic substrate potential, several numerical and asymptotic results have been obtained. The pioneering work on numerical simulation was carried out by Currie et al. [2] showing that an initial condition, which is the configuration of the exact one-kink solution of the continuous Sine-Gordon equation, changes its shape a little by shrinking and radiates phonons resulting in spontaneous damping of the kink motion. However, Currie et al. did not follow the evolution sufficiently long enough to observe in detail the final state of the initial travelling kink.

Ishimori and Munakata [3] obtained the first results on asymptotic approximation, they studied the discreteness effects on the dynamics of a Sine-Gordon kink in the Frenkel and Kontorova lattice using the MacLaughlin and Scott perturbation formalism, that is, they considered the continuous approximation of the Frenkel and Kontorova model (Sine-Gordon lattice equation) to all orders and they wrote the model equation as a perturbed continuous Sine-Gordon equation, the corrections are the perturbation. They showed that from the zeroth order a kink moves in a periodic potential field, also known as Peierls–Nabarro (PN) potential, which causes wobbling and pinning of the kink. However no attempt was made to compare the asymptotic with the numerical solution.

Peyrard and Kruskal [4] studied the kink's dynamics in the discrete Sine-Gordon equation in the very discrete regimen. They studied in detail the complicated numerical evolution of a travelling kink showing that all initial conditions have the same qualitative behavior. They discovered, solving the linearized Sine-Gordon equation with a forcing term given by the travelling kink, that the kink will emit radiation when its velocity resonates with the phase velocity of the lattice waves (phonons). This radiation was found to be large at large kink velocities and small at small velocities. Using this, they explored the position of the knees and obtained an estimated mean kink position. However no equations were proposed to couple the radiation and the kink motion. In the continuous version and for initial conditions which are not the exact kink solution, Smyth and Worthy [8] obtained the radiation loss by means of the momentum and energy conservation

* Corresponding address: Department of Mathematics and Statistics, 461 Humanities Bldg, MSC03 2150, 1 University of New Mexico, Albuquerque, NM 87131-0001, USA. Tel.: +1 (505) 277 4803; fax: +1 (505) 277 5505.
E-mail address: cisneros@math.unm.edu (L.A. Cisneros).

0167-2789/$ - see front matter © 2007 Elsevier B.V. All rights reserved.
doi:10.1016/j.physd.2007.08.005

equations of the continuum Sine-Gordon equation. They calculated the momentum loss of the kink to the radiated waves. The radiated waves were calculated in terms of the kink parameters obtaining a closed system of equations. Boesch et al. [5,6] introduced a collective-variable method using a projection-operator approach to study the emission of phonon radiation from a discrete Sine-Gordon kink, with this approach they explained the radiative effects and the kink evolution. They obtained good quantitative comparisons between their collective-variable approach and the full numerical solution proving that the collective-variable method is a good idea to describe the kink. However in their collective-variable approach they had to solve numerically all the differential equations to account for the radiation. Kevrekidis and Weinstein [7] used the normal forms to study the large time behavior of kink solution in the discrete Sine-Gordon equation for initial conditions which are small perturbation of a stable kink. They studied in detail the kink's internal modes for the static case and they coupled them nonlinearly to the radiation modes in the continuous spectrum.

In this paper we consider the complementary situation namely we develop a quantitative asymptotic theory for the kink propagation calculating the effect of the radiation shed by the kink. We use the discrete average Lagrangian as the counterpart of the one considered in [8]. In this approach the Poisson summation formula provides the Peierls–Nabarro potential responsible for the hopping of the kink along the lattice. We find that unlike the continuum case only static kink solutions are possible. We also show that approximately propagating solutions only exist for velocities smaller than a certain threshold which explains why fast kinks do not propagate long distances.

The coupling between the kink and the radiation is studied using the existence of the resonant radiation discovered in [4] produced by the kink motion. This radiation is calculated using a discrete type of WKB solution. A careful study of the numerical solution in the neighborhood of the kink reveals that the dynamical counterpart of the Goldstone static mode is responsible for a small scale asymmetry of the kink. This is shown to produce a larger Peierls–Nabarro potential which in turn produces larger accelerations. When all these effects are included a remarkable agreement between the numerical and the asymptotic solution is found.

The paper is organized as follows: Section 2 formulates the problem and describes the relevant behavior of previously known numerical solution which is relevant to this work. In Section 3 we present the averaged Lagrangian for the asymptotic kink evolution and we explain qualitatively the possible behaviors, the relevant calculations of this section are presented in Appendix A. In Section 4 we describe the effect of the radiation on the kink and derive the radiation damped modulation equations. The details of the discrete signalling problem are documented in Appendix B. Section 5 is devoted to the study of the effect of the Goldstone mode on the propagating kink. Finally, Section 6 is devoted to detailed comparison between the modulation solution, which takes into account the Goldstone mode, and the full numerical solution. In Section 7 we present our conclusions. The details of several laborious calculations are in Appendix C.

2. Statement of the problem and numerical solution

The equation of the motion for the Frenkel and Kontorova model, which describes a chain of harmonically coupled particles subjected to an external periodic substrate potential, is the following discrete Sine-Gordon equation

$$\ddot{y}_n = y_{n-1} - 2y_n + y_{n+1} - \frac{1}{d^2}\sin y_n, \quad -\infty < n < \infty \tag{1}$$

which is obtained from the Lagrangian,

$$L = \sum_{n=-\infty}^{\infty} \frac{\dot{y}_n^2}{2} - \frac{1}{2}(y_{n+1} - y_n)^2 - \frac{1}{d^2}(1 - \cos y_n), \tag{2}$$

where the constant d is the discreteness parameter, d large ($d \gg 1$) is the continuous limit and $d < 1$ is the discrete one, y_n is the relative displacement of particle n.

For d large Eq. (1) can be approximate by the continuous Sine-Gordon equation. This is seen multiplying Eq. (1) by d^2 and making the change in variables $\tau = t/d$, $x_n = n/d$ to obtain,

$$u_{\tau\tau} = u_{xx} - \sin u.$$

This equation can be solved exactly [9] using the inverse scattering method obtaining a one parameter family of kink solutions given by,

$$u(x, \tau) = 4\arctan\exp\left(-\frac{x - v\tau}{\sqrt{1 - v^2}}\right), \tag{3}$$

where the velocity $0 \le v \le 1$ is arbitrary.

The discrete equations of motion (1) are not exactly integrable, however, these equations can be solved [4] numerically. We now reconsider briefly the numerical solution to reproduce the relevant results needed for our work.

We solve numerically a finite number, N, of equations using a Runge–Kutta method with initial conditions obtained from (3), that is

$$y_n(t_0) = 4\arctan\exp\left(-\frac{n - \xi_0}{d\sqrt{1 - v_0^2}}\right), \tag{4}$$

$$\dot{y}_n(t_0) = \frac{2}{d\sqrt{1 - v_0^2}}\operatorname{sech}\left(-\frac{n - \xi_0}{d\sqrt{1 - v_0^2}}\right), \quad -N \le n \le N \tag{5}$$

where $\xi_0 = v_0 t_0$ at initial time $t = t_0$ and the boundary conditions are taken to be $y_{-N} = 2\pi$, $y_N = 0$.

To avoid boundary reflexion problems, we solve for a large number of particles (typically 40 000 particles) so that the trailing waves of the front wave do not reach the artificial boundary. We estimate the numerical evolution of the position $\xi(t)$ and velocity $v(t) = \dot{\xi}(t)$ using an interpolation for the

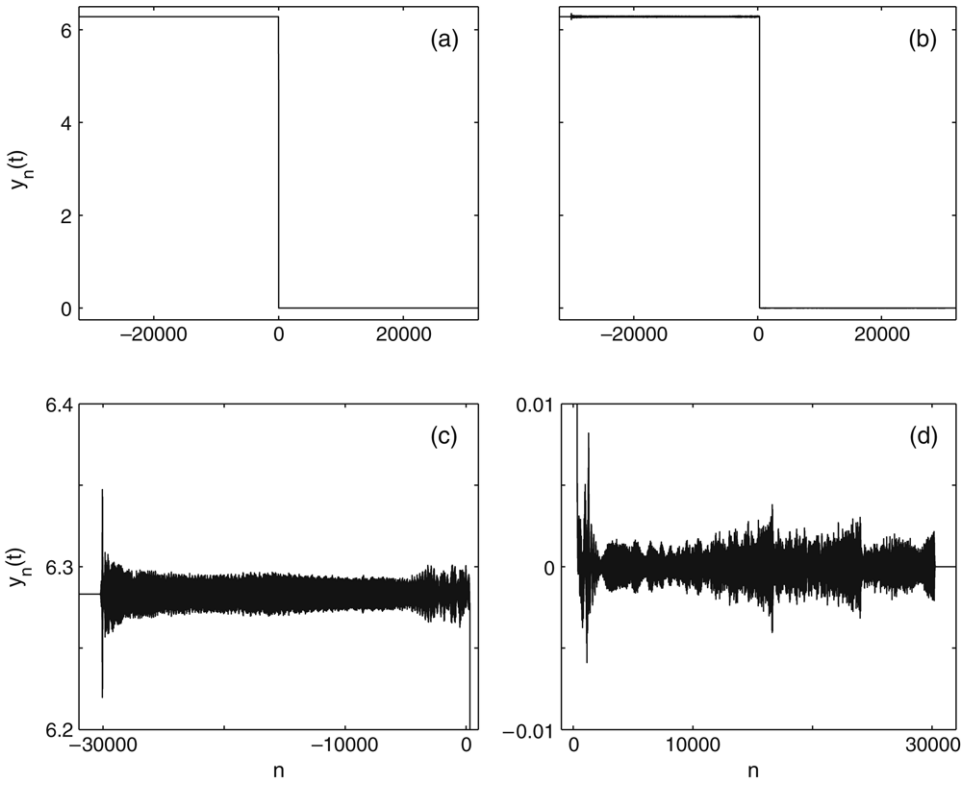

Fig. 1. Full numerical solution of system (1) for $2N+1$ particles with $v_0 = 0.8, \xi_0 = 0, d = 0.95, N = 32\,000$ and $\triangle t = 0.025$. (a) Initial condition (4), (b) numerical solution at $t = 50\,000$, (c) backward radiation and (d) forward radiation.

midpoint of the kink, as follows

$$\xi(t) \approx m + \frac{\pi - y_m(t)}{y_{m+1}(t) - y_m(t)}, \tag{6}$$

$$v(t) \approx \frac{\xi(t_{\text{new}}) - \xi(t_{\text{old}})}{\triangle t}, \tag{7}$$

where m is the integer that satisfies $y_m(t) > \pi$ and $y_{m+1}(t) < \pi$ at $t = t_{\text{new}}$ and $\triangle t = t_{\text{new}} - t_{\text{old}}$.

We reproduce the full numerical solution of Peyrard and Kruskal [4] for the initial conditions $v_0 = 0.8, \xi_0 = 0, d = 0.95$ and $v_0 = 0.4$, $\xi_0 = 0$, $d = 1$. The numerical evolution of the kink for the initial velocity $v_0 = 0.8$ is shown in Fig. 1. As described in [4], the kink decelerates very rapidly and after moving a relatively short distance in the lattice (to be contrasted with the travelling wave in the continuum [8]) it is trapped, see Figs. 2 and 3. Also, there are trailing waves emitted as radiation predominantly at the back of the travelling kink and there are critical velocities at which there is an abrupt change in the type of trailing waves emitted by the travelling kink, these critical velocities are identified with the corresponding velocities to the knees of the curve in Fig. 2. We followed the kink evolution until it becomes trapped also observing knees appearing at larger times.

The kink evolution for the initial velocity $v_0 = 0.4$ has the same qualitative behavior as the initial velocity $v_0 = 0.8$ (see Figs. 4–6), but there is a strong quantitative difference between the two cases. For larger initial velocity v_0 the kink is rapidly trapped while for smaller initial velocity v_0 the kink travels almost like a free kink and eventually it is trapped.

Several authors have studied the asymptotic of propagating kinks [3,10]. In these works the damping mechanisms have been discussed in a qualitative way and no quantitative results were obtained. In [4] the main mechanism of radiation damping is found but the detailed coupling of the radiation to the kink was not addressed. On the other hand, the asymptotic evolution of the trapped kink has been studied by Kevrekidis and Weinstein [7] and shown to be dominated by the nonlinear interaction of the internal kink modes with the radiation. We are interested in the complementary regime namely the asymptotic study of the kink dynamics before the trapping occurs. In particular, how the internal modes of the kink couple to the radiation loss during the hopping of the kink along the lattice.

3. Asymptotic equations for the kink evolution

Following Smyth and Worthy [8], who studied the kink evolution for the continuous Sine-Gordon equation, we take the modulated kink solution in the form:

$$y_n(t) = K_n(t) = 4 \arctan \exp\left(-\frac{n - \xi(t)}{w(t)}\right). \tag{8}$$

As in the continuum case, we assume that the width $w(t)$ of this trial function will adjust and the velocity $v(t) = \dot{\xi}(t)$ will be non-uniform, from the initial condition (4) we have $v(t_0) = v_0, \xi_0 = \xi(t_0) = v_0 t_0$, and $w(t_0) = d\sqrt{1 - v_0}$ at the initial time $t = t_0$. A previous study [10] assumed that w is

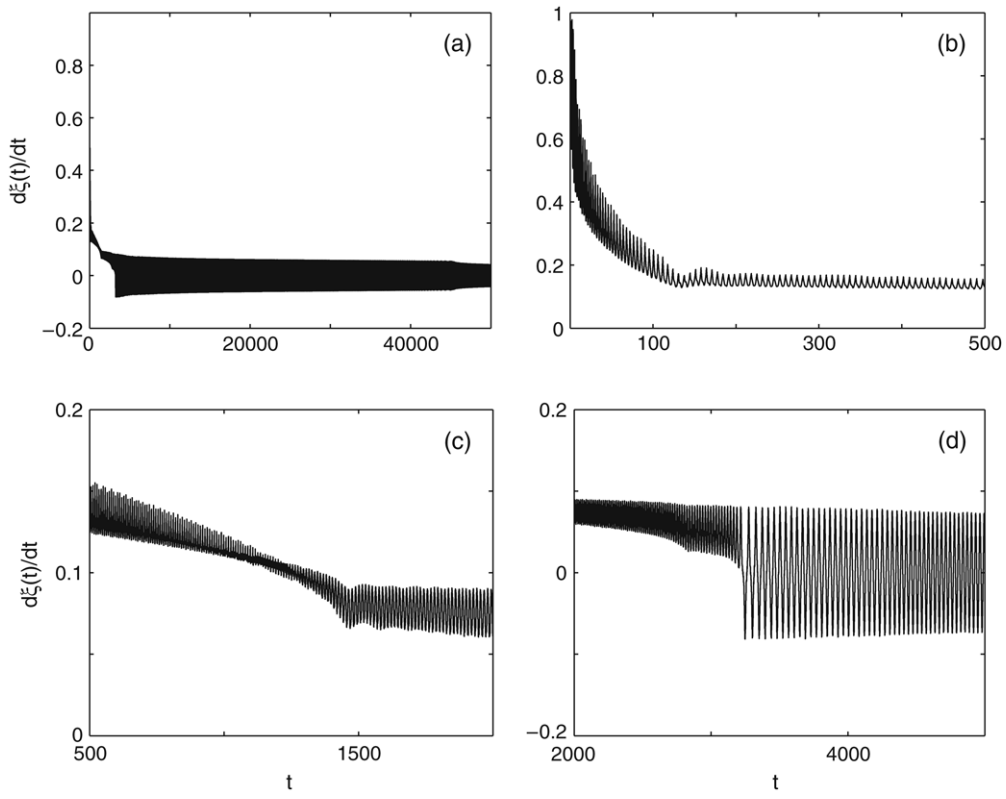

Fig. 2. (a) Numerical evolution of velocity (7) for $v_0 = 0.8, \xi_0 = 0, d = 0.95, N = 32\,000$ and $\triangle t = 0.025$ at $t = 50\,000$, (b) first knee, (c) second knee and (d) third knee and trapped velocity.

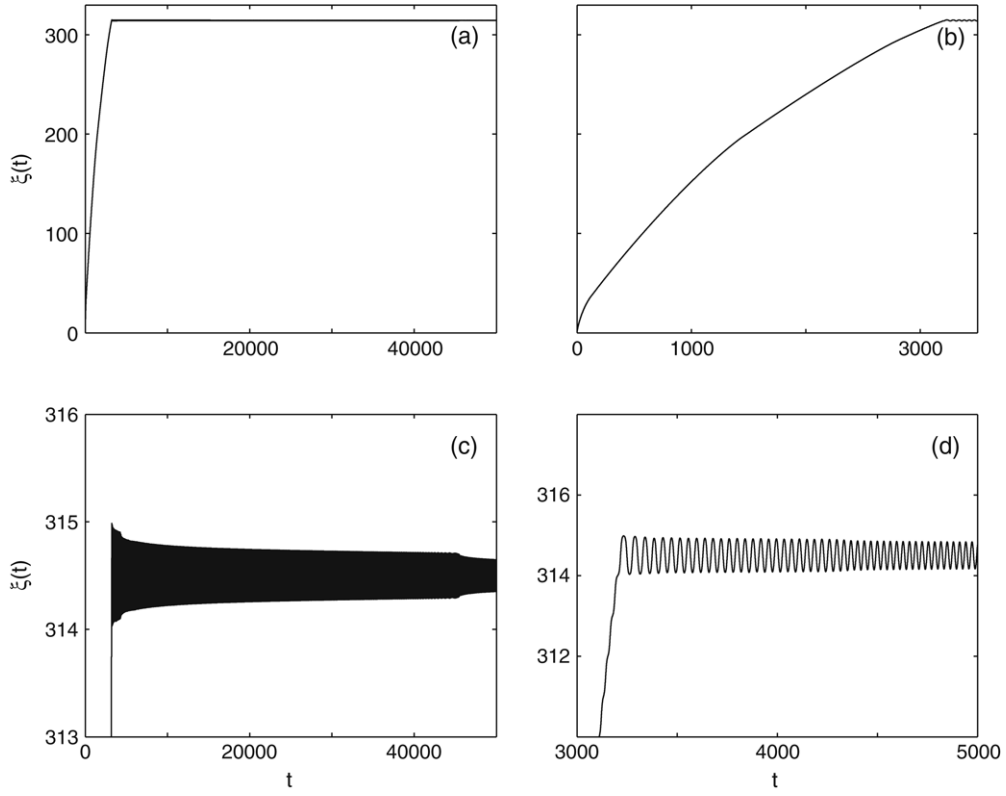

Fig. 3. (a) Numerical evolution of position (6) for $v_0 = 0.8, \xi_0 = 0, d = 0.95, N = 32\,000$ and $\triangle t = 0.025$ at $t = 50\,000$, (b) zoom of (a), (c) numerical position of trapped kink and (d) zoom of (c).

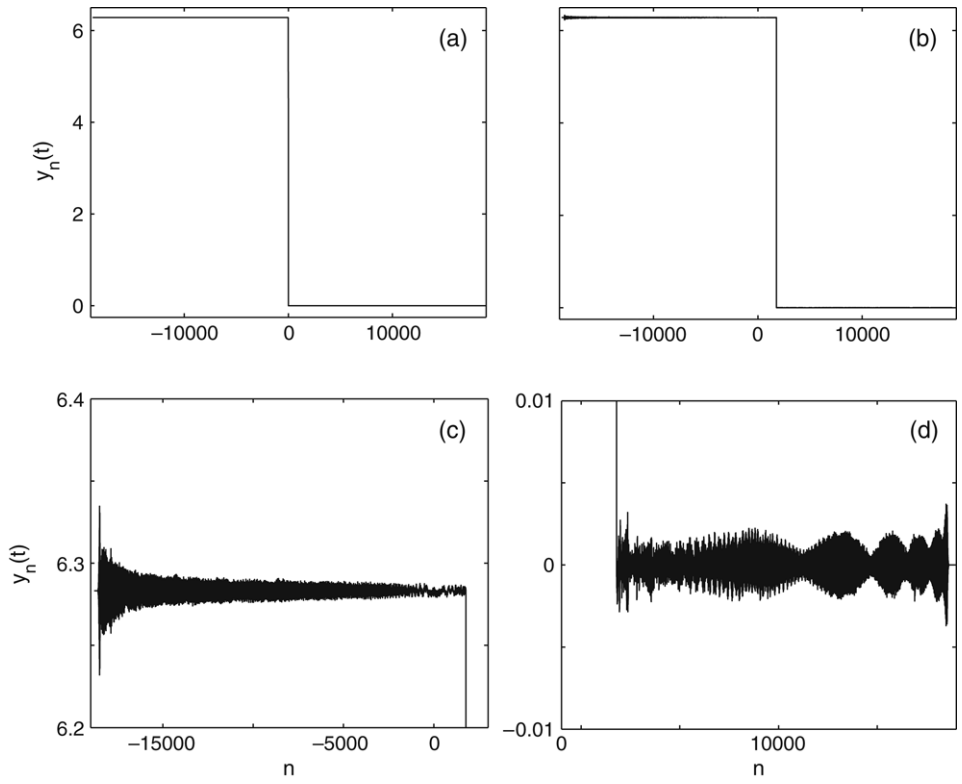

Fig. 4. Full numerical solution of system (1) for $2N+1$ particles with $v_0 = 0.4$, $\xi_0 = 0$, $d = 1$, $N = 20\,000$ and $\triangle t = 0.025$. (a) Initial condition (4), (b) numerical solution at $t = 30\,000$, (c) backward radiation and (d) forward radiation.

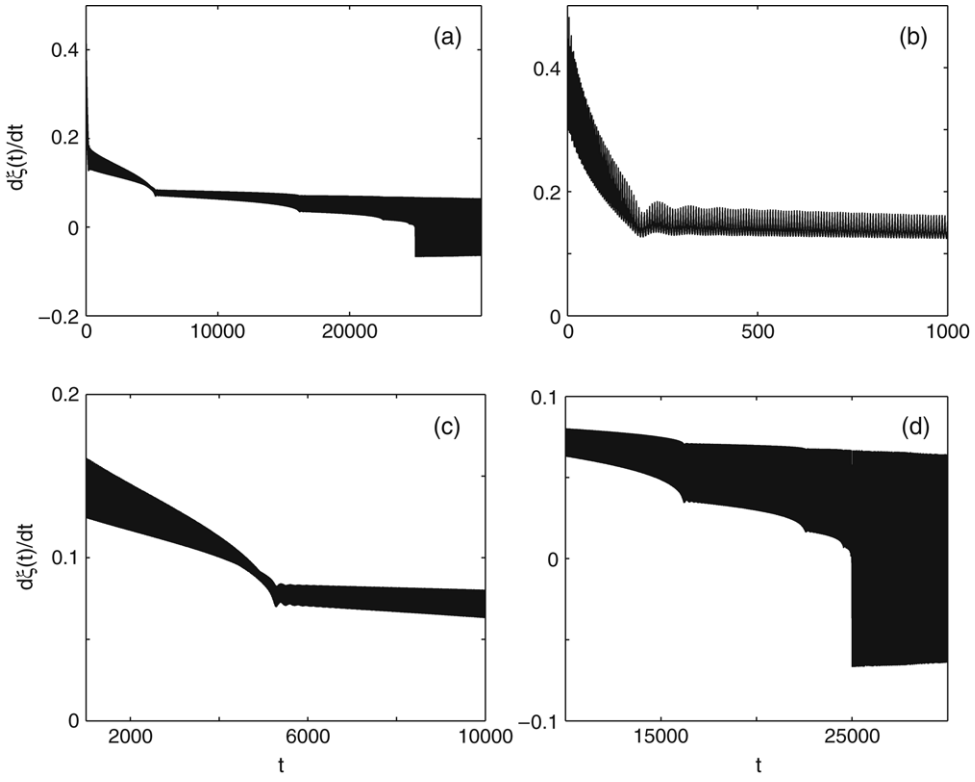

Fig. 5. (a) Numerical evolution of velocity (7) for $v_0 = 0.4$, $\xi_0 = 0$, $d = 1$, $N = 20\,000$ and $\triangle t = 0.025$ at $t = 30\,000$, (b) first knee, (c) second knee and (d) third knee and trapped velocity.

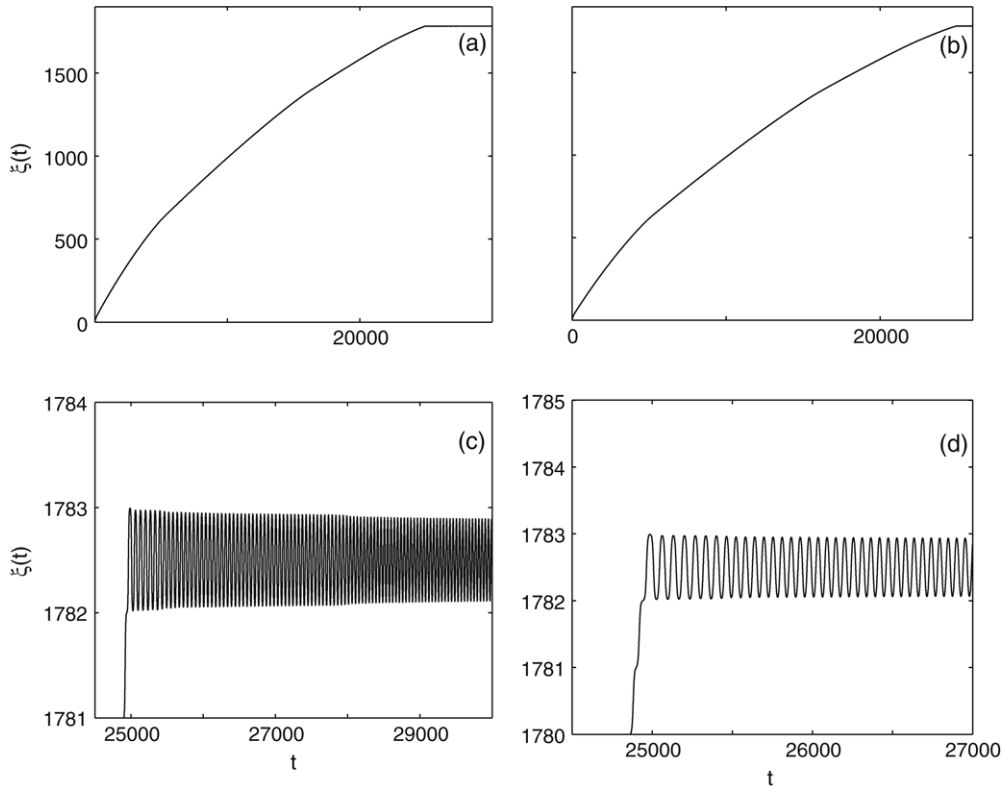

Fig. 6. (a) Numerical evolution of position (6) for $v_0 = 0.4, \xi_0 = 0, d = 1, N = 20\,000$ and $\triangle t = 0.025$ at $t = 30\,000$, (b) zoom of (a), (c) numerical position of trapped kink and (d) zoom of (c).

fixed and relatively large for the kink scattering by impurities in a discrete chain and no detailed quantitative comparison were given between numerics and asymptotics.

The trial function (8) is then substituted in the Lagrangian (2) to obtain the averaged Lagrangian

$$L = \left(\frac{2\dot{\xi}^2}{w^2} - \frac{2}{d^2}\right) \sum_{n=-\infty}^{\infty} \operatorname{sech}^2\left(\frac{n-\xi}{w}\right) + \frac{2\dot{w}^2}{w^2} \sum_{n=-\infty}^{\infty} \left(\frac{n-\xi}{w}\right)^2 \operatorname{sech}^2\left(\frac{n-\xi}{w}\right) - 8 \sum_{n=-\infty}^{\infty} \arctan^2\left(\sinh\frac{1}{2w} \operatorname{sech}\left(\frac{n-\xi}{w} + \frac{1}{2w}\right)\right), \quad (9)$$

where we have used the exact relations,

$$y_n - y_{n+1} = 4 \arctan\left(\sinh\frac{1}{2w} \operatorname{sech}\left(\frac{n-\xi}{w} + \frac{1}{2w}\right)\right),$$

$$\dot{y}_n = \frac{2}{w^2} \operatorname{sech}\left(\frac{n-\xi}{w}\right)\left(\dot{\xi}\, w + \dot{w}\,(n-\xi)\right),$$

$$1 - \cos y_n = 2 \operatorname{sech}^2\left(\frac{n-\xi}{w}\right).$$

The term proportional to $\dot{\xi}\,\dot{w}$ has been neglected because it does not contribute to the dynamics. To evaluate the Lagrangian (9), we observe that taking w relatively large (continuum approximation), we have

$$y_n - y_{n+1} \approx \frac{2}{w} \operatorname{sech}\left(\frac{n-\xi}{w}\right). \quad (10)$$

Using (10) in (9) and the Poisson summation formula (see Appendix A) we obtain to leading order

$$L = \left(\frac{\dot{\xi}^2}{w^2} - \frac{1}{d^2} - \frac{1}{w^2}\right) 4w + \frac{\pi^2 \dot{w}^2}{3w}, \quad (11)$$

which as expected recovers the Lagrangian obtained by Smyth and Worthy [8] for the continuous Sine-Gordon equation.

To find the effects due to the discreteness of the lattice we use the Poisson summation formula in the full expression (9). The details are given in Appendix A. Only the leading order periodic correction which is the Peierls–Nabarro (PN) potential is retained. We obtain

$$L_K = \left(\frac{2\dot{\xi}^2}{w^2} - \frac{2}{d^2}\right)\left(2w + \frac{4\pi^2 w^2}{\sinh\left(\pi^2 w\right)} \cos\left(2\pi\xi\right)\right) + \frac{\pi^2 \dot{w}^2}{3w} - h\,(w), \quad (12)$$

where

$$h\,(w) = 8 \int_{-\infty}^{\infty} \arctan^2\left(\sinh\frac{1}{2w} \operatorname{sech}\frac{x}{w}\right) \mathrm{d}x$$

can be interpolated as:

$$h(w) \approx \frac{28+120w}{1.4+6w+30w^2}, \quad \text{for } w > 0.$$

Notice that for $w \gg 1$, $h(w) \approx 4/w$ and Eq. (12) recovers the continuum limit.

The periodic PN terms are exponentially small when $w \gg 1$. On the other hand they have an important contribution when $w \approx 1$ which shows the strong lattice effects on the motion of the kink.

Taking variations in the averaged Lagrangian (12) with respect to ξ and w, we obtain the ordinary differential equations for the kink parameters

$$\delta\xi : \ddot{\xi} = \left(\dot{\xi}^2 + \frac{w^2}{d^2}\right) \frac{2\pi^3 w}{\sinh\left(\pi^2 w\right)} \sin(2\pi\xi), \tag{13}$$

$$\delta w : \ddot{w} = \frac{\dot{w}^2}{2w} - \frac{6w}{\pi^2 d^2} - \frac{6\dot{\xi}^2}{\pi^2 w} - \frac{3w}{2\pi^2} h'(w). \tag{14}$$

For fixed w and satisfying the continuum dispersion relation, $w = d\sqrt{1-\dot{\xi}^2}$, the first equation is the same one discussed by Braun and Kivshar [10] once the appropriate scaling and the approximation (10) are used. Eq. (13) has saddles in the nodes (particles) of the chain and centers in the middle of consecutive nodes. The unbounded orbits represent the jumping of the kink along the lattice. The equation for w displays the fact that w has no fixed point unless the kink itself is stationary and there are two possibilities, at a node or between two nodes, moreover notice that as expected the selection of the steady state is determined by exponentially small terms [7, 11]. This explains the numerical observation that all kink initial conditions become trapped. On the other hand if the PN potential is neglected we find that the equation for w has fixed points for,

$$R(w) = \dot{\xi}^2 \tag{15}$$

with

$$R(w) = -\frac{w^2}{4}\left(\frac{4}{d^2} + h'(w)\right). \tag{16}$$

In Fig. 7 we show a graph of (16). We observe that the discrete dispersion relation (15) is satisfied only if $0 \le \dot{\xi} \lesssim 0.7064$ for $d = 1$ which is in contrast with the continuous dispersion relation, $S(w) = 1 - w^2/d^2 = \dot{\xi}^2$, which can be satisfied for all $0 \le \dot{\xi} \le 1$. This explains why low velocity kinks propagate for longer distances since they are approximated fixed points and are within an exponentially small correction steady propagating solutions of the equations. On the other hand rapid kinks are not approximated steady propagating solutions. They must radiate a great quantity of energy to adjust to possible approximate kink solutions. To complete the modulation theory we must include the effect of radiation following [4,8].

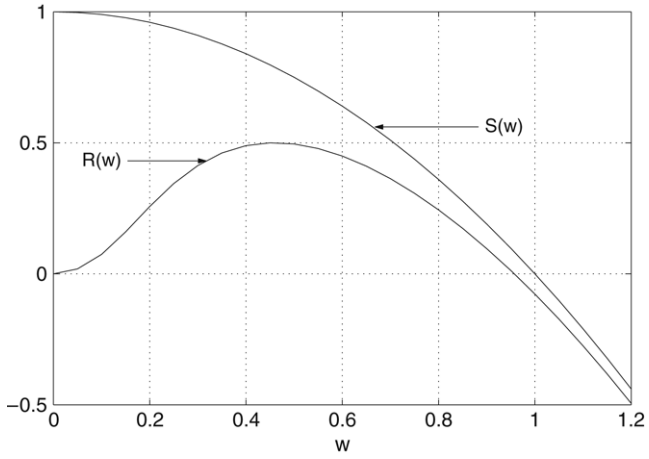

Fig. 7. Graphs of $R(w)$ related to the discrete dispersion relation (15) and $S(w) = 1 - w^2/d^2$ related to the continuous dispersion relation, both for $d = 1$.

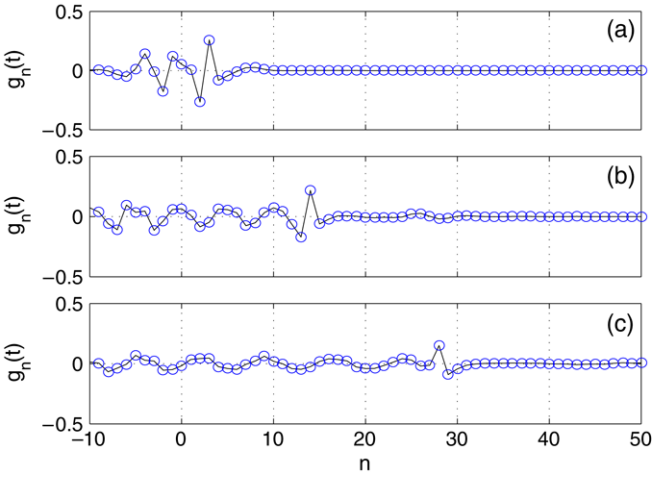

Fig. 8. Divided difference of $y_n^{\text{num}}(t) - K_n(t)$ between the full numerical solution and the modulated kink (8) using (6) and (7) to estimate the modulated parameters for (a) $t = 10$, (b) $t = 45$ and (c) $t = 100$.

4. The effect of radiation

To calculate the effect of radiation we calculate the energy loss proposed by Peyrard and Kruskal using the ideas of [8] to relate it to the motion of the kink. To this end the solution is assumed to be $y_n(t) \sim K_n(t)$ for $\xi - l \le n \le \xi + l$ where l is a suitable cut off node and $y_n^R(t) \sim y_n^c(t) + y_n^{PK}(t)$ outside the region occupied by the kink. This decomposition is suggested by the results in Fig. 8. In Fig. 8 the divided difference $g_n(t) = (y_{n+1}^{\text{num}}(t) - K_{n+1}(t)) - (y_n^{\text{num}}(t) - K_n(t))$ has two components. The first one is a relatively flat shelf which is produced by long wave radiation as in the continuum case to the readjustment of w. This is taken into account by $y_n^c(t)$. The Peyrard and Kruskal trailing wave radiation $y_n^{PK}(t)$ which is controlled by the leading peak in Fig. 8 is the one discussed in [4]. This radiation is absent in the continuum limit because it is caused by the resonance of the wave numbers $\omega/\dot{\xi}$ produced by the moving source with the lattice period for definite values of ω. With these assumptions the energy loss takes the form:

$$\frac{\mathrm{d}}{\mathrm{d}t}\sum_{n=\xi-l}^{\xi+l}\frac{\dot{y}_n^2}{2}+\frac{1}{2}\left(y_{n+1}-y_n\right)^2+\frac{1}{d^2}\left(1-\cos y_n\right)$$
$$=\dot{\xi}\left[\frac{\dot{y}_n^2}{2}+\frac{1}{2}\left(y_{n+1}-y_n\right)^2+\frac{1}{d^2}\left(1-\cos y_n\right)\right]_{\xi-l}^{\xi+l}$$
$$+\sum_{n=\xi-l}^{\xi+l}\dot{y}_n\ddot{y}_n+\left(y_{n+1}-y_n\right)\left(\dot{y}_{n+1}-\dot{y}_n\right)+\frac{\dot{y}_n}{d^2}\sin y_n. \tag{17}$$

Now the left hand side is evaluated at the coherent kink and (17) becomes

$$\frac{\mathrm{d}}{\mathrm{d}t}\left[\left(\frac{2\dot{\xi}^2}{w^2}+\frac{2}{d^2}\right)\left(2w+\frac{4\pi^2w^2}{\sinh\left(\pi^2w\right)}\cos\left(2\pi\xi\right)\right)\right.$$
$$\left.+\frac{\pi^2\dot{w}^2}{3w}+h\left(w\right)\right]=-\left[\dot{y}_n^R\left(y_{n+1}^R-y_n^R\right)\right]_{\xi-l}^{\xi+l}, \tag{18}$$

where we have assumed a symmetric radiation shedding due to the small velocity. Since the radiation is small we calculate y_n^R using the linearized equation.

$$\ddot{y}_n^R-\left(y_{n-1}^R-2y_n^R+y_{n+1}^R\right)+\frac{1}{d^2}y_n^R=0, \tag{19}$$

with an appropriate signalling boundary condition, which is discussed in Appendix B, on y_n^R at the leading and trailing edges of the kink. From Eq. (38) of the Appendix B, we obtain:

$$\left[\dot{y}_n^c\,\partial y_n^c/\partial n\right]_{\xi-l}^{\xi+l}=\frac{\pi^2\dot{w}^2}{3c_gwt} \tag{20}$$

and from Eq. (46), we have

$$-\left[\dot{y}_n^{PK}\,\partial y_n^{PK}/\partial n\right]_{\xi-l}$$
$$=-\sum_k 128\pi^2\left|R\left(w_k\right)\right|^2\exp\left(-\frac{\pi w_k}{v}w\rho\right)$$
$$\times\frac{w_k^2}{v^3}\cos^2\left(\frac{w_k}{v}\left(\xi+l\right)+w_kt+\psi_k\right). \tag{21}$$

The average of Eq. (21) is the energy loss studied in [4]. The cross products between y_n^c and y_n^{PK} do not contribute since we average on the fast time scale to obtain:

$$\frac{\mathrm{d}}{\mathrm{d}t}\left[\left(\frac{2\dot{\xi}^2}{w^2}+\frac{2}{d^2}\right)\left(2w+\frac{4\pi^2w^2}{\sinh\left(\pi^2w\right)}\cos\left(2\pi\xi\right)\right)\right.$$
$$\left.+\frac{\pi^2\dot{w}^2}{3w}+h\left(w\right)\right]=-\frac{\pi^2\dot{w}^2}{3c_gwt}-\sum_k 64\pi^2\left|R\left(w_k\right)\right|^2$$
$$\times\exp\left(-\frac{\rho\pi ww_k}{v}\right)\frac{w_k^2}{v^3}. \tag{22}$$

Since the average of $|R(w_k)|$ is approximately v, we obtain:

$$\frac{8}{w}\left[\ddot{\xi}-\left(\dot{\xi}^2+\frac{w^2}{d^2}\right)\frac{2\pi^3w}{\sinh\left(\pi^2w\right)}\sin\left(2\pi\xi\right)\right]\dot{\xi}$$
$$+\frac{2\pi^2}{3w}\left[\ddot{w}-\frac{\dot{w}^2}{2w}+\frac{6w}{\pi^2d^2}+\frac{6\dot{\xi}^2}{\pi^2w}+\frac{3w}{2\pi^2}h'\left(w\right)\right]\dot{w}$$
$$=-\frac{\pi^2\dot{w}^2}{3c_gwt}-\sum_k 64\pi^2\exp\left(-\frac{\rho\pi ww_k}{v}\right)\frac{w_k^2}{v}.$$

Since $\dot{w}=0$ during the oscillation to obtain a non-singular equation, we equate the energy loss of w to the equation of motion of w to obtain

$$\ddot{w}-\frac{\dot{w}^2}{2w}+\frac{6w}{\pi^2d^2}+\frac{6\dot{\xi}^2}{\pi^2w}+\frac{3w}{2\pi^2}h'\left(w\right)=-\frac{\dot{w}}{2c_gt} \tag{23}$$

and

$$\ddot{\xi}-\left(\dot{\xi}^2+\frac{w^2}{d^2}\right)\frac{2\pi^3w}{\sinh\left(\pi^2w\right)}\sin\left(2\pi\xi\right)$$
$$=-\dot{\xi}\sum_k 8\pi^2w\exp\left(-\frac{\rho\pi ww_k}{v}\right)\frac{w_k^2}{v^3}. \tag{24}$$

Notice that in Eq. (24) the resonant damping is not of the form $\mu\dot{\xi}$ with μ constant. It depends on $v=\dot{\xi}$ to capture the fact that for large velocities the damping is relatively large due to the smallness of $w_k/\dot{\xi}$. However as $\dot{\xi}$ decreases, as is discussed in [4] and is described in Appendix B, $w_k/\dot{\xi}$ grows and the equation $\frac{1}{d^2}+2-2\cos(\frac{w_k}{v})=w_k^2$ losses the small roots w_k. This produces the knee in the velocity evolution since the damping decreases abruptly when the small roots are lost. Notice that this form of damping goes to zero as $\dot{\xi}\to 0$, which is to be expected since the kink does not resonate with the lattice as it becomes steady.

Before we compare the solution of (23) and (24) with the corresponding full numerical solution, we analyze qualitatively the nature of the modulational solutions. In Eq. (24) the damping decreases $\dot{\xi}$, thus the width w given by (23) adjusts to a new larger value (the kink becomes broader) as $\dot{\xi}$ decreases. This in turn lowers the PN potential barrier. This allows the kink to propagate for relatively long distances since it settles onto an approximately propagating solution of (23) and (24).

In Figs. 9–12 we show a comparison between the full numerical solution and the modulational solution with kink parameters evolving according to (23) and (24). In the Figs. 9 and 10 we show the comparisons for $\rho=0.925$ in the radiation damping. We note from Figs. 9 and 10 that for constant $\rho=0.925$ we have a very good comparison with the full numerical solution up to the time of the first knee. We observe that there is a relatively large acceleration. This process, as we discuss in Appendix B, cannot be obtained analytically since there are no explicit analytic solutions for the signalling problem

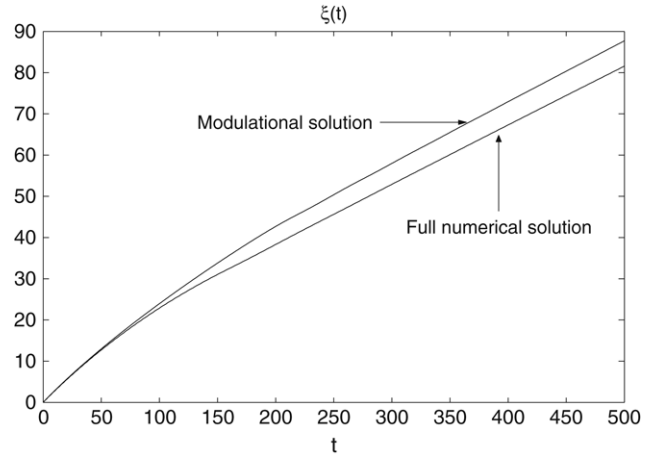

Fig. 9. Numerical comparison between the numerical position (6) and the solution of the system (23) and (24) for $\rho = 0.925$ and $v_0 = 0.3$.

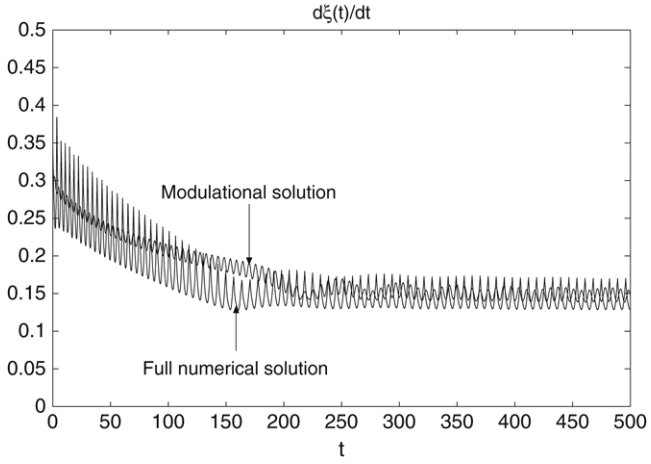

Fig. 10. Numerical comparison between the numerical velocity (7) and the solution of the system (23) and (24) for $\rho = 0.925$ and $v_0 = 0.3$.

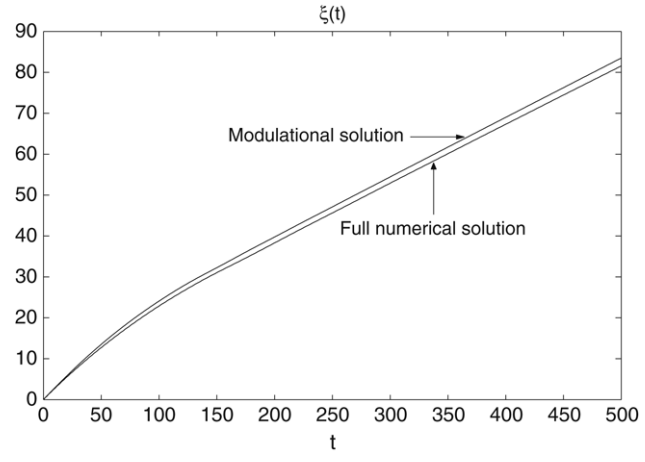

Fig. 11. Numerical comparison between the numerical position (6) and the solution of the system (23) and (24) for $\rho(t) = 1 - 0.15\tanh(t/60)$ and $v_0 = 0.3$.

with variable velocity v. We thus take the change in ρ to be of the form $\rho(t) = 1 - 0.15\tanh(t/60)$ which has the correct time scale ($t \approx 60$) for the first knee and account for the mismatch between $\xi(t)$ and $\dot{\xi}\,t$. The results obtained are shown in Figs. 11 and 12 and are indeed very good. It is to be remarked that the same function $\rho(t)$ is used for a variety of initial conditions obtaining very good agreement with mean for initial velocities between 0.3 and 0.5. A closer comparison shows that the oscillation of the modulation equations is smaller than the numerical one (see Fig. 13). This is because the PN potential barrier is very sensitive to the width of the kink due to its exponential dependence. This discrepancy suggests that unlike the continuous problem where the comparison is very good there is another mechanism which accounts for the larger oscillations. We now describe how the dynamical counterpart of the internal modes, studied in [7] for the static case, accounts for the larger oscillations.

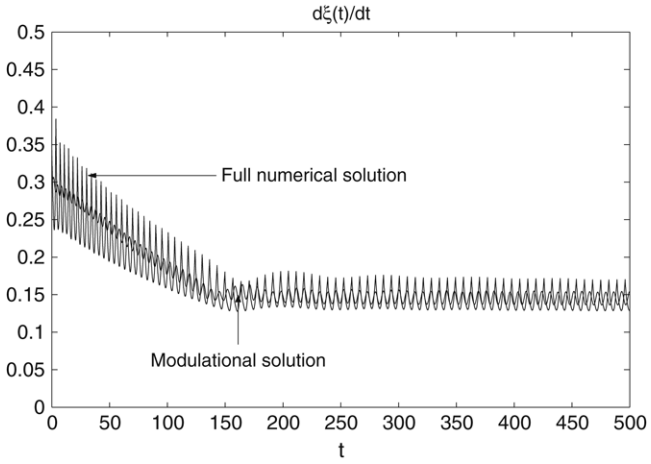

Fig. 12. Numerical comparison between the numerical velocity (7) and the solution of the system (23) and (24) for $\rho(t) = 1 - 0.15\tanh(t/60)$ and $v_0 = 0.3$.

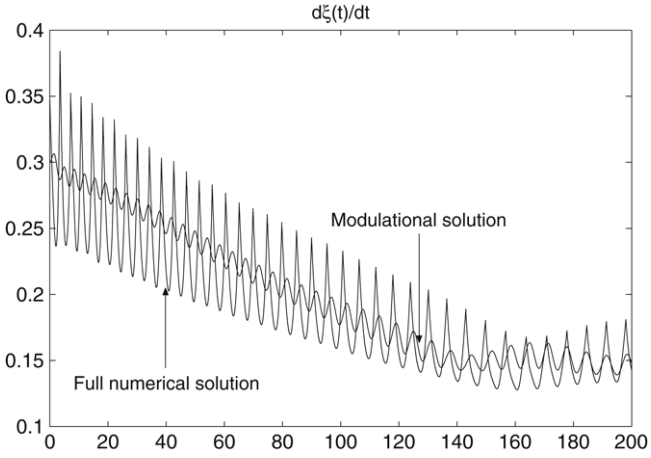

Fig. 13. Numerical comparison of Fig. 12 in a smaller window.

5. The dynamical effect of the internal modes

The static discrete kink has internal modes as established by Kevrekidis and Weinstein [7]. There is an edge mode [7] with eigenvalue close to the lower edge of the continuum band

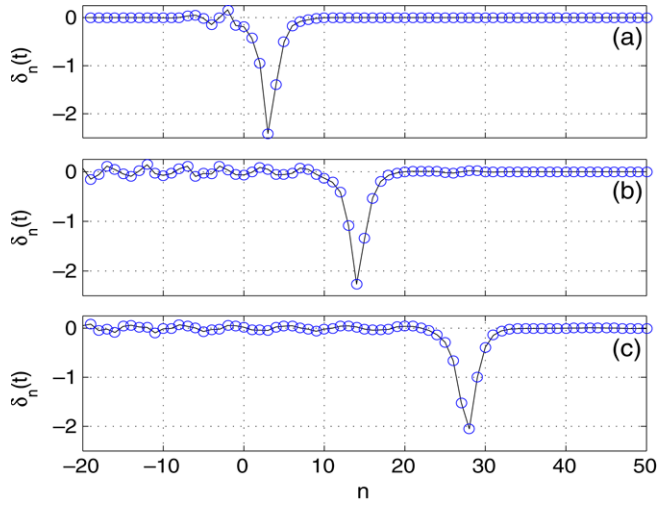

Fig. 14. Graph of (27) showing the asymmetry of the peak for (a) $t = 10$, (b) $t = 45$ and (c) $t = 100$.

gap, $\pm i(\frac{1}{d}, \sqrt{4+\frac{1}{d^2}})$. There is also a Goldstone mode which is the counterpart of the zero eigenvalue mode given in the continuum limit by the phase derivative of the kink solution due to the translation invariance. In the discrete case the translation invariance is lost and the zero eigenvalue of the continuum problem becomes an exponentially small eigenvalue for the discrete case. Moreover, this eigenvalue can be positive or negative depending on the kink's position. The Goldstone mode can be taken to leading order [7] to be $A\,\mathrm{sech}((n-\xi)/\lambda)$. To study the dynamical effect of this mode we observe from Fig. 14 that the peak of the divided difference

$$\delta_n(t) = y_{n+1}^{\mathrm{num}}(t) - y_n^{\mathrm{num}}(t) \tag{25}$$

has an asymmetry which evolves in time. On the other hand,

$$\triangle_n(t) = K_{n+1}(t) - K_n(t) \tag{26}$$

has no asymmetry. Thus the difference,

$$g_n(t) = \triangle_n(t) - \delta_n(t) \tag{27}$$

which is plotted in Fig. 8 is the asymmetry in the peak. From Fig. 8 we observe that the larger g_n is located at the kink location and it is a dipole. This has the same form of the divided difference of the Goldstone mode. Moreover, this mode is seen to interact strongly with the radiation. Thus for the modulation theory we take a trial function which includes a modulation of the Goldstone mode in the form:

$$y_n(t) = 4\arctan\exp\left(-\frac{n-\xi(t)}{w(t)}\right) + A(t)\,\mathrm{sech}\left(\frac{n-\xi(t)}{\lambda(t)}\right). \tag{28}$$

The effect of the edge mode is accounted for by the time dependence of $w(t)$. Using (28) we obtain the averaged Lagrangian in the form,

$$L = L_K + L_A + L_{\mathrm{int}}. \tag{29}$$

The Lagrangian L_K is the previously studied kink Lagrangian (12).

The Lagrangian L_A corresponds to the internal mode. Since the amplitude A is assumed to be small (see Fig. 8), we have from Appendix C

$$\begin{aligned} L_A = {} & \lambda\dot{A}^2 + \frac{\dot{\lambda}^2 A^2}{36\lambda}\left(12+\pi^2\right) \\ & + \frac{\dot{\xi}^2 A^2}{2\lambda^2}\left(\frac{2\lambda}{3} + \frac{\lambda^2\left(1-2\pi^2\lambda^2\right)}{6\sinh\left(\pi^2\lambda\right)}\cos(2\pi\xi)\right) \\ & - A^2\left(2\lambda - \frac{2}{\sinh\frac{1}{\lambda}} - 4\lambda I_1(\lambda)\cos(2\pi\xi)\right) \\ & - \frac{A^2}{2d^2}\left(2\lambda - \frac{5.5\lambda w}{1.1w+\lambda} + 4\cos(2\pi\xi)\right. \\ & \left.\times\left(\frac{\pi^2\lambda^2}{\sinh\left(\pi^2\lambda\right)} - I_2(\lambda, w)\right)\right) \\ & + \frac{A^4}{24d^2}\left(\frac{4}{3}\lambda - 2.132w^{0.2}\lambda^{0.8} + 4\cos(2\pi\xi)\right. \\ & \left.\times\left(\frac{2\pi^2\lambda^2\left(1+\pi^2\lambda^2\right)}{3\sinh\left(\pi^2\lambda\right)} - I_3(\lambda, w)\right)\right). \end{aligned} \tag{30}$$

The functions $I_1(\lambda)$, $I_2(\lambda, w)$ and $I_3(\lambda, w)$ are given in the Appendix C. As expected the quadratic terms of L_A involve the PN contribution which in the static case is responsible for the change in stability of the kink depending on its position. The effect of the dynamics is included in the terms $\dot{\lambda}^2$ and $\dot{\xi}^2$. The interaction terms in L_{int} are of two types. One gives the added mass to the kink due to the internal mode and the second type of interaction produces a modification of the PN potential, $V(w, \lambda)$, felt by the kink due to the presence of the internal mode. This interaction will be shown to be responsible for the enhancement of the oscillation in velocity described in the previous section. This last Lagrangian is calculated in Appendix C in the form,

$$\begin{aligned} L_{\mathrm{int}} = {} & \frac{4A\sin(2\pi\xi)}{\lambda w}\left(\dot{\xi}^2 - 1\right)V(w, \lambda) \\ & - \frac{4A}{d^2}\sin(2\pi\xi)\,V(\lambda, w) + \frac{2A^3}{3d^2}\sin(2\pi\xi)\,S(\lambda, w). \end{aligned} \tag{31}$$

Thus the dynamical effect of the internal mode is obtained by solving the modulation equations given by the Lagrangian (29). There will be new equations for A and λ, the equation for w will be also modified. The equation for the position will now have a larger PN potential due to the interaction with the internal mode which will be shown to explain the larger amplitude of the numerical velocity oscillation which was not captured using only the kink trial function. In detail the equations take the form:

$$\ddot{\xi} - 4w\pi^3\exp(-\pi^2 w)\left(\dot{\xi}^2 + \frac{w^2}{d^2}\right)\sin(2\pi\xi)$$

$$+\frac{\pi}{\lambda}A\left(\dot{\xi}^2+1\right)V(w,\lambda)\cos(2\pi\xi)$$
$$+\frac{\pi w}{d^2}AV(\lambda,w)\cos(2\pi\xi)-\frac{\dot{\xi}\dot{w}}{w}=l_\xi \tag{32}$$

$$\ddot{w}-\frac{\dot{w}^2}{2w}+\frac{6}{\pi^2 w}\left(\dot{\xi}^2+\frac{w^2}{d^2}\right)+\frac{3w}{2\pi^2}h'(w)$$
$$-\frac{5.9676A^2\lambda^2 w}{2\pi^2 d^2\left(\lambda^2-0.0156\lambda w+2.0376w^2\right)}$$
$$+\frac{0.4264A^4 w^{0.2}\lambda^{0.8}}{16\pi^2 d^2}=l_w \tag{33}$$

$$\ddot{A}-A\left[\dot{\lambda}^2\frac{(12+\pi^2)}{36\lambda^2}+\frac{\dot{\xi}^2}{3\lambda^2}-2+\frac{2}{\lambda\sinh\frac{1}{\lambda}}+\frac{1.65w-\lambda}{d^2(1.1w+\lambda)}\right]$$
$$-\frac{A^3}{d^2}\left[\frac{1}{9}-\frac{2.132}{12}\left(\frac{w}{\lambda}\right)^{0.2}\right]=l_A \tag{34}$$

$$\ddot{\lambda}-\frac{\dot{\lambda}^2}{2\lambda}+\frac{6\dot{\xi}^2}{\lambda\left(12+\pi^2\right)}-\frac{18\lambda\dot{A}^2}{A^2\left(12+\pi^2\right)}$$
$$+\frac{36}{\lambda\left(12+\pi^2\right)}\left(\lambda^2-\frac{\cosh\frac{1}{\lambda}}{\sinh^2\frac{1}{\lambda}}\right)$$
$$+\frac{18\lambda}{d^2\left(12+\pi^2\right)}\left(1-\frac{1.9892w^2}{w^2-0.0156\lambda w+2.0376\lambda^2}\right)$$
$$-\frac{A^2\lambda}{d^2\left(12+\pi^2\right)}\left(1-1.2792\left(\frac{w}{\lambda}\right)^{0.2}\right)=l_\lambda. \tag{35}$$

The loss for the ξ equation is basically as before because the contribution of the Goldstone mode is very small (see Fig. 8). We thus have:

$$l_\xi=-\dot{\xi}\sum_k 8\pi^2 w\exp\left(-\frac{\rho\pi w w_k}{v}\right)\frac{w_k^2}{v^3}$$

$$l_w=-\frac{\dot{w}}{2c_g t},$$

$$l_A=-\frac{\dot{A}}{2c_g t},$$

$$l_\lambda=-\frac{\dot{\lambda}}{2c_g t}.$$

These modulation equations will now be used to explain quantitatively the kink dynamics using simple interaction description between the modulated kink and the internal mode generated by its motion through the lattice.

6. Solution to the modulation equations and comparison with the full numerical results

Before we compare the solution of modulational equations with the full numerical solution we describe quantitatively the behavior of these modulation solutions. The equation for w has a center at the right root of the discrete dispersion relation (15) and the width of the kink is attracted toward this steady state due to the damping. On the other hand, the equation for λ has a center for $\lambda=0.85$ and a saddle for $\lambda=0.35$ when $w=0.9$. This center is to be expected since it corresponds to the minimum of the Rayleigh quotient as a function of λ for the trial function approximating the Goldstone mode. The equation for A has a critical point for $A=0$. The linear part at this point has two terms. The first one gives the value of the static Rayleigh quotient which alternates sign depending on whether the kink is at a minimum or a maximum for the PN potential. The second term is the dynamic modification of this behavior due to the terms $\dot{\xi}^2$ and $\dot{\lambda}^2$. We thus see that due to the rapid oscillation of the kink parameters this term will have a small average. It will turn out that the average is small and negative. Thus, the $A=0$ fixed point is a center with a long time scale. The A^3 term prevents the run away of the amplitude of the internal mode during the unstable part of the eigenvalue cycle covered by the hopping of the kink.

Finally, the equation for the ξ has a new term in the PN potential proportional to A caused by the internal mode. This term is important since the integral in $V(\lambda,w)$ involves a double pole which gives a relatively large contribution. Due to the long period of A this contribution is important for a long time. As before the change in the damping produces the knee taking into account the internal mode. This analysis explains qualitatively in simple terms the behavior of the travelling kink in the lattice.

We now compare the modulational solution with the numerical results. We use for the comparison $\rho(t)=1-0.15\tanh(t/60)$. We now see that the amplitude agreement is very good due to the influence of the internal mode. As shown in Figs. 15–17. The same $\rho(t)$ was used for other initial conditions and Figs. 18 and 19 display the velocity comparisons for $v_0=0.4$ and $v_0=0.5$, respectively. We see that the agreement is remarkable due to the complexity of the radiation process and the approximation used. At later stages after the first knee the radiation damping of the approximate equations is too strong and the modulation theory for the radiation cannot capture the details of the abrupt change in the radiation. Beyond the first knee the PN barrier becomes small and since the damping is also small the kink travels as a continuum kink for a small velocity.

7. Discussion and conclusions

We have developed a modulation solution including the radiation for the motion of a Sine-Gordon kink in a discrete lattice. We have shown that unlike the continuum case not even approximate kink solutions are possible for a velocity $\dot{\xi}>\dot{\xi}_c=0.7064$. This explains why fast initial kinks radiate a great deal of energy to adjust to approximate travelling kinks with smaller velocity. For smaller velocities the dynamics of the kink can be accurately studied including the evolution of the two internal modes. The effect of the edge mode is captured (as in the continuum case) by the modulation of the kink width and the flat shelf radiation. The effect of the

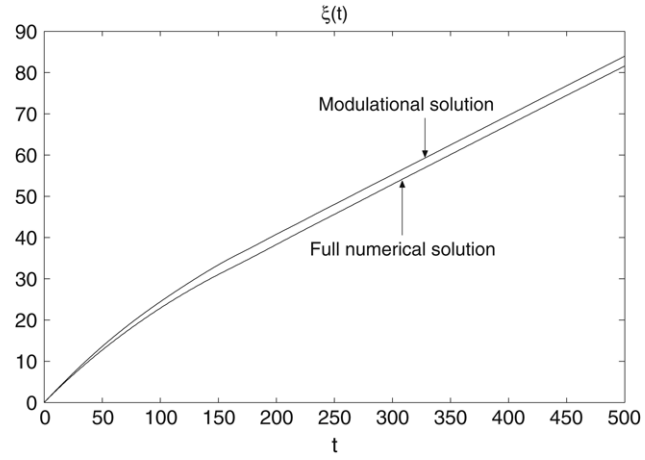

Fig. 15. Numerical comparison between the numerical position (6) and the solution of the system (32)–(35) for $\rho(t) = 1 - 0.15\tanh(t/60)$ and $v_0 = 0.3$.

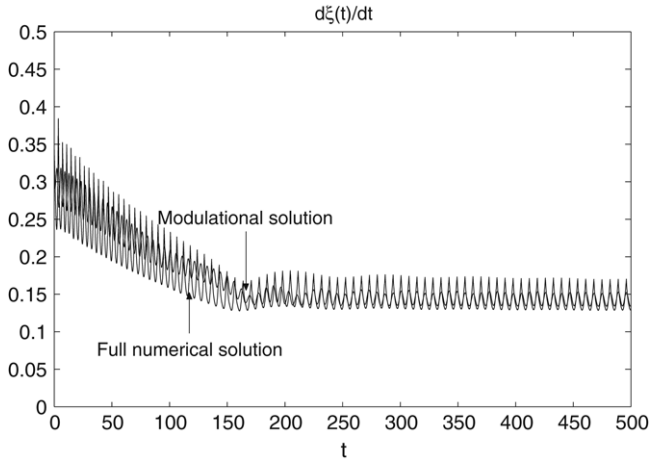

Fig. 16. Numerical comparison between the numerical velocity (7) and the solution of the system (32)–(35) for $\rho(t) = 1 - 0.15\tanh(t/60)$ and $v_0 = 0.3$.

Goldstone mode is taken into account explicitly. The effect of the discrete Goldstone mode is of crucial importance since the kink travels jumping between a stable and an unstable state, at the minimum and maximum of the PN potential. As the internal mode grows or oscillates, the shape of the kink develops a narrow asymmetry. This in turn is responsible for the modification of the PN potential increasing its value due to the small scale contribution. This enhances the velocity oscillation and the resonant radiation.

The radiation mechanism discovered by Peyrard and Kruskal [4] was incorporated in detail into the modulational solution to give the damping term which was not calculated in the previous studies. This was calculated by solving approximately an appropriately defined signalling problem for the linear discrete equation using a discrete analogue of the superposition of WKB type solutions.

With these simple mechanisms we explained in very good quantitative detail the dynamics of the kink before setting into an equilibrium. We also observe that the equations for fixed ξ are analogous to the ones studied by Kevrekidis and Weinstein [7]. However, the higher order interactions that

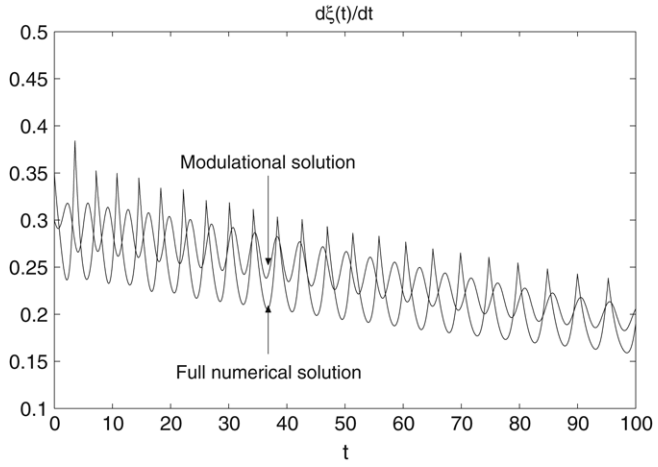

Fig. 17. Numerical comparison between the numerical velocity (7) and the solution of the system (32)–(35) for $\rho(t) = 1 - 0.15\tanh(t/60)$ and $v_0 = 0.3$ in a smaller window.

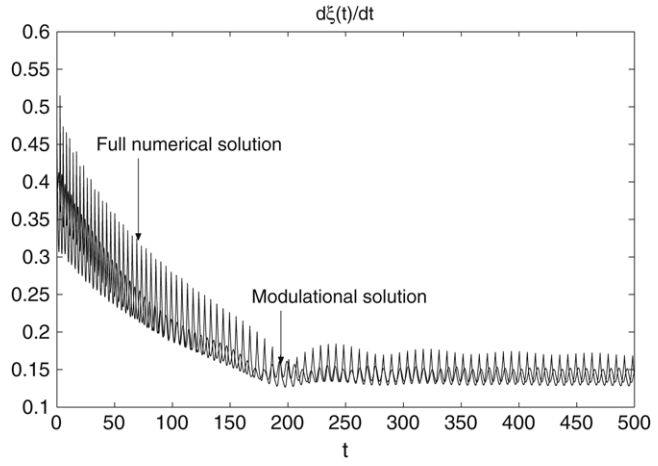

Fig. 18. Numerical comparison between the numerical velocity (7) and the solution of the system (32)–(35) for $\rho(t) = 1 - 0.15\tanh(t/60)$ and $v_0 = 0.4$.

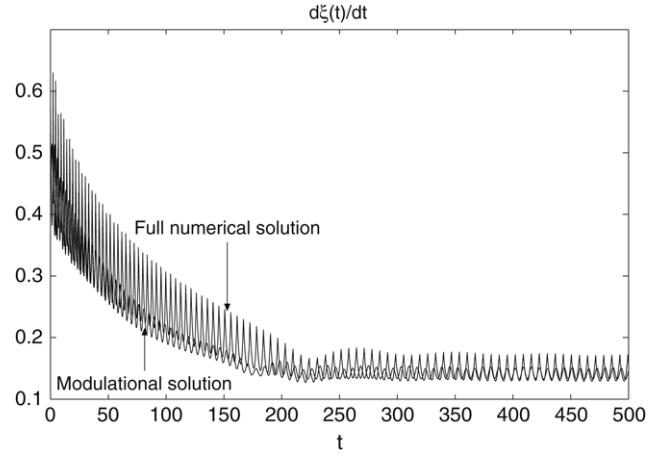

Fig. 19. Numerical comparison between the numerical velocity (7) and the solution of the system (32)–(35) for $\rho(t) = 1 - 0.15\tanh(t/60)$ and $v_0 = 0.5$.

we neglected between the kink, the internal modes and the radiation in the dynamics become important in this regime. The

equations for the transition between the moving kink studied in this work and the static kink studied in [7] need to be developed to capture the transition between the different behaviors of the radiation. This delicate question needs to be studied in further work. In particular, how to incorporate the small knees of Figs. 2 and 5 will require a more precise analysis of the radiation.

We conclude by remarking how the modulation solution explains in simple terms the mechanism which couple the kink with the internal modes and the radiation. This approach gives a simple and accurate asymptotic method which can be used in other situations involving kink propagation in lattices.

Acknowledgements

The authors would like to express their gratitude to Noel F. Smyth for advice concerning the full numerical solution, to Panayotis Panayotaros for useful discussions and to Cristobal Vargas for getting them interested in lattices. Also, they would like to thank the anonymous reviewer for the comments. L. A. Cisneros gratefully acknowledges support from the grant CONACYT-No.Reg.170517 from the Consejo Nacional de Ciencia y Tecnologia Mexico and the grant SNI-Exp763 from the Sistema Nacional de Investigadores.

Appendix A

For an analytic function $f(x)$ the Poisson summation formula takes the form:

$$\sum_{n=-\infty}^{\infty} f\,(n-\xi) = \frac{1}{2}A_0 + \sum_{n=1}^{\infty} A_n \cos\left(2n\pi\xi\right) + \sum_{n=1}^{\infty} B_n \sin\left(2n\pi\xi\right),$$

where

$$A_n = 2\int_{-\infty}^{\infty} f\,(z)\cos\left(2n\pi z\right)\mathrm{d}z, \quad n = 0, 1, 2, \ldots$$

$$B_n = 2\int_{-\infty}^{\infty} f\,(z)\sin\left(2n\pi z\right)\mathrm{d}z, \quad n = 0, 1, 2, \ldots.$$

The coefficients, A_n and B_n which are exponentially small in the width of f, control the size of the PN potential barrier.

To leading order this formula gives,

$$\begin{aligned}\sum_{n=-\infty}^{\infty} \operatorname{sech}^2\left(\frac{n-\xi}{w}\right) &= 2w + \frac{4\pi^2 w^2}{\sinh\left(\pi^2 w\right)}\cos\left(2\pi\xi\right)\\ &\quad \sum_{n=-\infty}^{\infty}\left(\frac{n-\xi}{w}\right)^2 \operatorname{sech}^2\left(\frac{n-\xi}{w}\right)\\ &= \frac{\pi^2 w}{6} - \frac{\pi^4 w^2\cos\left(2\pi\xi\right)}{2\sinh^3\left(\pi^2 w\right)}\\ &\quad \times\left(3+\cosh\left(2\pi^2 w\right) - \frac{2}{w\pi^2}\sinh\left(2\pi^2 w\right)\right)\\ &\quad \sum_{n=-\infty}^{\infty}\arctan^2\left(\sinh\frac{1}{2w}\operatorname{sech}\left(\frac{n-\xi}{w}+\frac{1}{2w}\right)\right)\\ &= \frac{3.5+15w}{1.4+6w+30w^2} + 2w\cos\left(2\pi\xi\right)\\ &\quad \times\int_{-\infty}^{\infty}\arctan^2\left(\sinh\frac{1}{2w}\operatorname{sech}\left(x+\frac{1}{2w}\right)\right)\cos\left(2\pi x\right)\mathrm{d}x.\end{aligned}$$

The first term in the last sum is obtained by means of an interpolation of the corresponding integral, which cannot be calculated in closed form. The rest of the terms are at most $O(\mathrm{e}^{-2\pi^2 w})$.

Appendix B. Radiation damping

B.1. The long wave radiation emitted by the shelf

Long waves generated by the shelf are assumed to satisfy the linear continuous Sine-Gordon equation with the boundary condition $u_x = g\,(t)$ at $x = \xi\,(t)$, as in [8]. The boundary condition $g\,(t)$ is determined, equating the excess of energy contained in the coherent structure with the energy contained in the radiation shed. For the kink, the excess of kinetic energy in w obtained from the linearization of L_K (12) at the fixed point w_0 gives,

$$\frac{\pi^2\dot{w}^2}{3w_0} = \frac{1}{2}\int_{-c_g t+(\xi-l)}^{c_g t+(\xi+l)}\left(u_t^2+u_x^2+u^2\right)\mathrm{d}x, \tag{36}$$

where c_g is the group velocity of the linear waves obtained from the linearized equation $\ddot{y}_n - (y_{n-1} - 2y_n + y_{n+1}) + \frac{1}{d^2}y_n = 0$. That is,

$$c_g = \frac{\sin\left(k\right)}{\sqrt{1/d^2 + 4\sin^2\left(k/2\right)}} \tag{37}$$

with k as the wave number. The wave number k is estimated by considering the frequency Ω of the linear oscillator for w at the fixed point. Thus the waves are produced at a wave number k which satisfies $w\,(k) = \Omega$, $w\,(k) = \sin^2\left(k/2\right)$. This gives $c_g \approx 1/10$.

Since $u_x = g$ at the boundary, then the integral (36) is estimated by the trapezoidal rule to obtain (see [8]),

$$g^2 = \frac{\pi^2\dot{w}^2}{3c_g w_0 t^2}.$$

As in [8], this gives

$$\left[\dot{y}_n^c\,\partial y_n^c/\partial n\right]_{\xi-l}^{\xi+l} = g^2 t = \frac{\pi^2\dot{w}^2}{3c_g w_0 t}. \tag{38}$$

In the case of the internal mode the excess energy includes the kinetic energy of the internal in mode L_A which is,

$$\lambda\dot{A}^2 + \frac{\dot{\lambda}^2 A^2}{36\lambda}\left(12+\pi^2\right).$$

Thus in the general case, we have

$$\left[\dot{y}_n^c\,\partial y_n^c/\partial n\right]_{\xi-l}^{\xi+l}$$

$$= \frac{1}{c_g t}\left(\frac{\pi^2 \dot{w}^2}{3w_0} + \lambda_0 \dot{A}^2 + \frac{\dot{\lambda}^2 A^2}{36\lambda_0}\left(12+\pi^2\right)\right). \tag{39}$$

B.2. The Peyrard and Kruskal radiation

The Peyrard and Kruskal radiation is caused by the resonance of the kink motion with the lattice. To determine its effect we need to solve,

$$\ddot{y}_n^{PK} - \left(y_{n-1}^{PK} - 2y_n^{PK} + y_{n+1}^{PK}\right) + \frac{1}{d^2} y_n^{PK} = 0, \quad n \le \xi(t) \tag{40}$$

with appropriate matching conditions to the kink for $n \approx \xi(t)$. From Fig. 8 we observe that this type of radiation is produced by the oscillation of the spatial difference of the kink. Thus a suitable difference of y_n^{PK} must be matched to a given function $f(n-\xi(t))$, which is determined by the shape of the difference of the kink and of the internal modes which are also excited, as n approaches $\xi(t)$. Clearly this problem has no exact solution. Moreover, we need to derive a suitable matching condition in order to calculate the radiation. To this end we begin by studying the Laplace transform of the boundary condition in the form:

$$\int_0^\infty f(n-\xi(t))\, e^{-st} dt.$$

The integral cannot be evaluated in closed form. We thus take $\xi(t) \approx vt$ where $v = \dot{\xi}$, since we expected the deviation $\xi - vt$ to be small. In this case the integral can be evaluated by assuming v to be constant, since it is slowly varying, to obtain:

$$\frac{1}{v} e^{-ns/v} \int_{-n}^\infty e^{-su/v} f(-u)\, du = e^{-ns/v} B(s,n)$$

$$B(s,n) = \frac{1}{v}\int_{-n}^\infty e^{-su/v} f(-u)\, du. \tag{41}$$

The boundary condition (41) for (40) has a WKB form since for small vB is slowly varying and the phase in the exponential has large variations in n. We then take a WKB type of solution $A(n,s)\exp\varphi(n,s)$ for the Laplace transform of Eq. (40),

$$\left(s^2 + 2 + \frac{1}{d^2}\right)\tilde{y}_n^{PK} - \left(\tilde{y}_{n-1}^{PK} + \tilde{y}_{n+1}^{PK}\right) = 0.$$

To leading order the phase $\varphi(n,s)$ satisfies the discrete dispersion relation,

$$\left(s^2 + 2 + \frac{1}{d^2}\right) - \left(\exp(\varphi(n+1,s) - \varphi(n,s)) + \exp(\varphi(n-1,s) - \varphi(n,s))\right) = 0.$$

Assuming $\varphi(n+1,s) - \varphi(n,s) \approx \varphi'(n,s)$, we obtain $\varphi'(n,s) = \ln\lambda(s)$, where $\lambda(s)$ is the root of $(s^2 + 2 + \frac{1}{d^2}) - \lambda + \lambda^{-1} = 0$. This gives the appropriate wave number of the discrete lattice at $s = iw$. The function $A(n,s)$ will be determined in the matching.

A suitable matching condition is obtained choosing the point $n = N \approx \xi$, and the points $n = N+1$ and $n = N-1$. Fig. 8 suggests matching the spatial difference of the radiation to the spatial difference of the kink, thus we take the derivative to be $(u(N+1) - u(N-1))/2$ and it is to be matched to $e^{-ns/v} B(s,n)$. This gives

$$u(N+1) - u(N-1) = 2Be^{-Ns/v}$$

$$A(s)\left(\exp(\varphi(N+1,s) - \varphi(N,s)) - \exp(\varphi(N-1,s) - \varphi(N,s))\right) = 2Be^{-Ns/v}.$$

For matching, we take $\varphi(N) = -Ns/v$ and $\varphi(N+1) = -(N+1)s/v$ in the kink region. On the other hand $-\varphi(N) + \varphi(N-1)$ is the radiation region and it satisfies the dispersion relation. Which gives $\exp(\varphi(N-1) - \varphi(N)) = \lambda^{-1}(s)$.

We thus determine $A(n,s)$ in the form:

$$A(n,s) = \frac{2B}{e^{-s/v} - \lambda^{-1}(s)}. \tag{42}$$

The approximate solution takes the form:

$$y_n(t) = \frac{1}{2\pi i}\int_C \lambda^n(s)\frac{2B}{e^{-s/v} - \lambda^{-1}(s)} e^{st} ds. \tag{43}$$

The contour C lies in $\mathrm{Re}\, s > 0$. The singularities of the integrand are two branch points extending from $\pm i\sqrt{4 + \frac{1}{d^2}}$ to infinity. The poles are at the roots of the dispersion relation $\lambda(s) = e^{s/v}$ which recovers the resonant waves described in [4] as the dominant contribution to the solution (the function v is assumed slowly varying). The poles are on the imaginary axis and give real residues in the form:

$$y_n(t) = \sum_k e^{inw_k/v} e^{iwt}\frac{2B(iw_k)}{-e^{-iw_k/v}/v + \lambda'/\lambda^2} + c.c, \tag{44}$$

where the sum extends on the roots w_k of $e^{-s/v} - \lambda^{-1}(s) = 0$ as in [4]. Notice that the waves move to the left, also as v goes to zero the small roots w_k are lost as described in [4]. To complete the solution we calculate $B(iw_k)$.

We have

$$B(iw_k) = \frac{1}{v}\int_{-N}^\infty e^{iw_k u/v} f(-u)\, du.$$

Since N is relatively large compared to the width of the even $f(u)$. Then we can take,

$$B(iw_k) = \frac{1}{v}\int_{-\infty}^\infty e^{iw_k u/v} f(-u)\, du. \tag{45}$$

The function $f(u)$ is provided by the derivative of the kink shape (see Eq. (8)) and the integral is extended to $-\infty < u < \infty$. In this case $f(u) = -\frac{2}{w}\,\mathrm{sech}\left(\frac{u}{w}\right)$. This integral is exponentially small since it is controlled by the poles of $f(-u)$ in $\mathrm{Im}\, w < 0$. Finally, we must take into account the fact that $\frac{x-\xi(t)}{w}$ is not $\frac{x-vt}{w}$. In fact we have from Fig. 9 that $\frac{x-vt}{w} < \frac{x-\xi(t)}{w}$. On the other hand the functional dependence $x - vt$ is needed to construct the approximate solution for the radiation. Because of this we approximate $\frac{x-\xi(t)}{w}$ by $\frac{x-vt}{\rho w}$ where ρ is a slowly varying function. To determine ρ we note from

Fig. 9 that ρ is basically constant and not too different from 1 except at the point of larger acceleration which is at the knee. Moreover, this point is well-estimated using a constant value of $\rho \approx 1$. We thus propose a decreasing ρ to adjust the mismatch with a decrease around $t = 60$ which is the time of the first knee estimated from the $\rho = 1$ solution to the modulation equations. The actual values in $\rho(t) = 1 - 0.15\tanh(t/60)$ were estimated by fitting, as in other problems, the result to a specific initial condition of $v = 0.4$. Then similar results were obtained with the same $\rho(t)$ for a range of initial velocities between 0.3 and 0.5. It is to be noted that this approach ties the proposed modification of the width in [4] to the details of the radiation mechanism. This shows that for discrete problems since there are larger accelerations at the knee, the effect of the radiation is more sensitive to the exact position of the kink than in the continuous case, where $\rho = 1$ is sufficient since there are no knees [8].

We finally obtain estimating $B(\mathrm{i}w_k)$ by the residue at the first pole in the form,

$$B(\mathrm{i}w_k) = -\frac{4\pi}{v}\exp\left(-\frac{\pi w_k}{2v}w\rho\right). \tag{46}$$

Using this expression into (44) we obtain,

$$y_n^{PK}(t) = -\sum_k \frac{8\pi}{v}\exp\left(-\frac{\pi w_k}{2v}w\rho\right)R(w_k) \times \cos\left(\frac{w_k}{v}n + w_k t + \psi_k\right), \tag{47}$$

where

$$R(w_k) = \frac{\left|\lambda^2(\mathrm{i}w_k)\right| v}{\left|\lambda'(\mathrm{i}w_k) - \lambda^2 \mathrm{e}^{-\mathrm{i}w_k/v}\right|}, \tag{48}$$

$$\psi_k = \arg\left(1/\left(\lambda'(\mathrm{i}w_k)/\lambda^2(\mathrm{i}w_k) - \mathrm{e}^{-\mathrm{i}w_k/v}\right)\right). \tag{49}$$

Appendix C

From the trial function (28) it is obtained

$$y_n - y_{n+1} = 4\arctan\left(\sinh\frac{1}{2w}\operatorname{sech}\left(\frac{n-\xi}{w}+\frac{1}{2w}\right)\right) + \frac{2A\sinh\frac{1}{2\lambda}\operatorname{sech}\left(\frac{n-\xi}{\lambda}+\frac{1}{2\lambda}\right)\tanh\left(\frac{n-\xi}{\lambda}+\frac{1}{2\lambda}\right)}{1+\sinh^2\frac{1}{2\lambda}\operatorname{sech}^2\left(\frac{n-\xi}{\lambda}+\frac{1}{2\lambda}\right)},$$

$$\dot{y}_n = \frac{2}{w^2}\operatorname{sech}\left(\frac{n-\xi}{w}\right)\left(\dot{\xi}w + \dot{w}(n-\xi)\right) + \dot{A}\operatorname{sech}\left(\frac{n-\xi}{\lambda}\right) + \frac{A}{\lambda^2}\left(\dot{\xi}\lambda + \dot{\lambda}(n-\xi)\right) \times \operatorname{sech}\left(\frac{n-\xi}{\lambda}\right)\tanh\left(\frac{n-\xi}{\lambda}\right),$$

$$1-\cos y_n \approx 2\operatorname{sech}^2\left(\frac{n-\xi}{w}\right) + 2A\operatorname{sech}\left(\frac{n-\xi}{\lambda}\right) \times \operatorname{sech}\left(\frac{n-\xi}{w}\right)\tanh\left(\frac{n-\xi}{w}\right) + \frac{A^2}{2}\left(\operatorname{sech}^2\left(\frac{n-\xi}{\lambda}\right) - 2\operatorname{sech}^2\left(\frac{n-\xi}{\lambda}\right)\operatorname{sech}^2\left(\frac{n-\xi}{w}\right)\right) - \frac{A^3}{3}\operatorname{sech}^3\left(\frac{n-\xi}{\lambda}\right)\operatorname{sech}\left(\frac{n-\xi}{w}\right)\tanh\left(\frac{n-\xi}{w}\right) - \frac{A^4}{24}\left(\operatorname{sech}^4\left(\frac{n-\xi}{\lambda}\right) - 2\operatorname{sech}^4\left(\frac{n-\xi}{\lambda}\right)\operatorname{sech}^2\left(\frac{n-\xi}{w}\right)\right),$$

where the last expression has been expanded in Taylor series as a function of A, near $A = 0$.

By substituting the last expressions into the Lagrangian (2) and neglecting the cross product of derivatives (for example: $\dot{\xi}\dot{w}, \ldots$) because they are smaller terms, it is found that the averaged Lagrangian is,

$$L = L_K + L_A + L_{\mathrm{int}},$$

where

$$L_K = \frac{2}{w^2}\left(\dot{\xi}^2 - \frac{w^2}{d^2}\right)\sum_{n=-\infty}^{\infty}\operatorname{sech}^2\left(\frac{n-\xi}{w}\right) + \frac{2\dot{w}^2}{w^2}\sum_{n=-\infty}^{\infty}\left(\frac{n-\xi}{w}\right)^2\operatorname{sech}^2\left(\frac{n-\xi}{w}\right) - 8\sum_{n=-\infty}^{\infty}\arctan^2\left(\sinh\frac{1}{2w}\operatorname{sech}\left(\frac{n-\xi}{w}+\frac{1}{2w}\right)\right),$$

$$L_A = \frac{\dot{A}^2}{2}\sum_{n=-\infty}^{\infty}\operatorname{sech}^2\left(\frac{n-\xi}{\lambda}\right) + \frac{\dot{\lambda}^2A^2}{2\lambda^2}\sum_{n=-\infty}^{\infty}\left(\frac{n-\xi}{\lambda}\right)^2 \times \operatorname{sech}^2\left(\frac{n-\xi}{\lambda}\right)\tanh^2\left(\frac{n-\xi}{\lambda}\right) + \frac{\dot{\xi}^2A^2}{2\lambda^2}\sum_{n=-\infty}^{\infty}\operatorname{sech}^2\left(\frac{n-\xi}{\lambda}\right)\tanh^2\left(\frac{n-\xi}{\lambda}\right) - A^2\sum_{n=-\infty}^{\infty}\frac{2\sinh^2\frac{1}{2\lambda}\operatorname{sech}^2\left(\frac{n-\xi}{\lambda}+\frac{1}{2\lambda}\right)\tanh^2\left(\frac{n-\xi}{\lambda}+\frac{1}{2\lambda}\right)}{\left(1+\sinh^2\frac{1}{2\lambda}\operatorname{sech}^2\left(\frac{n-\xi}{\lambda}+\frac{1}{2\lambda}\right)\right)^2} - \frac{A^2}{2d^2}\left(\sum_{n=-\infty}^{\infty}\operatorname{sech}^2\left(\frac{n-\xi}{\lambda}\right) - 2\sum_{n=-\infty}^{\infty}\operatorname{sech}^2\left(\frac{n-\xi}{\lambda}\right)\operatorname{sech}^2\left(\frac{n-\xi}{w}\right)\right) + \frac{A^4}{24d^2}\left(\sum_{n=-\infty}^{\infty}\operatorname{sech}^4\left(\frac{n-\xi}{\lambda}\right) - 2\sum_{n=-\infty}^{\infty}\operatorname{sech}^4\left(\frac{n-\xi}{\lambda}\right)\operatorname{sech}^2\left(\frac{n-\xi}{w}\right)\right),$$

and

$$L_{\mathrm{int}} = \frac{2A\dot{\xi}^2}{\lambda w}\sum_{n=-\infty}^{\infty}\operatorname{sech}\left(\frac{n-\xi}{w}\right)\operatorname{sech}\left(\frac{n-\xi}{\lambda}\right)\tanh\left(\frac{n-\xi}{\lambda}\right)$$

$$
\begin{aligned}
&- \frac{2A}{d^2} \sum_{n=-\infty}^{\infty} \operatorname{sech}\left(\frac{n-\xi}{\lambda}\right) \operatorname{sech}\left(\frac{n-\xi}{w}\right) \tanh\left(\frac{n-\xi}{w}\right) \\
&- A \sum_{n=-\infty}^{\infty} 8 \arctan\left(\sinh\frac{1}{2w} \operatorname{sech}\left(\frac{n+1/2-\xi}{w}\right)\right) \\
&\times \frac{\sinh\frac{1}{2\lambda} \operatorname{sech}\left(\frac{n+1/2-\xi}{\lambda}\right) \tanh\left(\frac{n+1/2-\xi}{\lambda}\right)}{1+\sinh^2\frac{1}{2\lambda} \operatorname{sech}^2\left(\frac{n+1/2-\xi}{\lambda}\right)} \\
&+ \frac{A^3}{3d^2} \sum_{n=-\infty}^{\infty} \operatorname{sech}^3\left(\frac{n-\xi}{\lambda}\right) \operatorname{sech}\left(\frac{n-\xi}{w}\right) \tanh\left(\frac{n-\xi}{w}\right).
\end{aligned}
$$

The series appearing in these Lagrangians are evaluated with the Poisson summation formula, and to leading order we obtain

$$
\begin{aligned}
&\sum_{n=-\infty}^{\infty} \operatorname{sech}\left(\frac{n-\xi}{w}\right) \operatorname{sech}\left(\frac{n-\xi}{\lambda}\right) \tanh\left(\frac{n-\xi}{\lambda}\right) \\
&= 2\sin(2\pi\xi) \int_{-\infty}^{\infty} \operatorname{sech}\frac{x}{w} \operatorname{sech}\frac{x}{\lambda} \tanh\frac{x}{\lambda} \sin(2\pi x)\,\mathrm{d}x \\
&= 2\sin(2\pi\xi)\, V(w,\lambda) \\
&\quad \sum_{n=-\infty}^{\infty} \operatorname{sech}^3\left(\frac{n-\xi}{\lambda}\right) \operatorname{sech}\left(\frac{n-\xi}{w}\right) \tanh\left(\frac{n-\xi}{w}\right) \\
&= 2\sin(2\pi\xi) \int_{-\infty}^{\infty} \operatorname{sech}^3\frac{x}{\lambda} \operatorname{sech}\frac{x}{w} \tanh\frac{x}{w} \sin(2\pi x)\,\mathrm{d}x \\
&= 2\sin(2\pi\xi)\, S(w,\lambda) \\
&\quad \sum_{n=-\infty}^{\infty} \operatorname{sech}^2\left(\frac{n-\xi}{\lambda}\right) \tanh^2\left(\frac{n-\xi}{\lambda}\right) \\
&= \frac{2\lambda}{3} + \frac{\lambda^2\left(1-2\pi^2\lambda^2\right)}{6\sinh\left(\pi^2\lambda\right)} \cos(2\pi\xi) \\
&\quad \sum_{n=-\infty}^{\infty} \left(\frac{n-\xi}{\lambda}\right)^2 \operatorname{sech}^2\left(\frac{n-\xi}{\lambda}\right) \tanh^2\left(\frac{n-\xi}{\lambda}\right) \\
&= \lambda\frac{12+\pi^2}{18} + 2\lambda\cos(2\pi\xi) \\
&\quad \times \int_{-\infty}^{\infty} x^2 \operatorname{sech}^2 x \tanh^2 x \cos(2\pi x\lambda)\,\mathrm{d}x \\
&\quad \sum_{n=-\infty}^{\infty} \frac{2\sinh^2\frac{1}{2\lambda} \operatorname{sech}^2\left(\frac{n-\xi}{\lambda}+\frac{1}{2\lambda}\right) \tanh^2\left(\frac{n-\xi}{\lambda}+\frac{1}{2\lambda}\right)}{\left(1+\sinh^2\frac{1}{2\lambda} \operatorname{sech}^2\left(\frac{n-\xi}{\lambda}+\frac{1}{2\lambda}\right)\right)^2} \\
&= 2\lambda - \frac{2}{\sinh\frac{1}{\lambda}} \\
&\quad - 4\lambda\cos(2\pi\xi) \int_{-\infty}^{\infty} \frac{\sinh^2\frac{1}{2\lambda} \operatorname{sech}^2 x \tanh^2 x \cos(2\pi\lambda x)}{\left(1+\sinh^2\frac{1}{2\lambda} \operatorname{sech}^2 x\right)^2}\mathrm{d}x \\
&= 2\lambda - \frac{2}{\sinh\frac{1}{\lambda}} - 4\lambda I_1(\lambda)\cos(2\pi\xi) \\
&\quad \sum_{n=-\infty}^{\infty} \operatorname{sech}^4\left(\frac{n-\xi}{\lambda}\right) \\
&= \frac{4}{3}\lambda + \frac{8\pi^2\lambda^2\left(1+\pi^2\lambda^2\right)}{3\sinh\left(\pi^2\lambda\right)} \cos(2\pi\xi) \\
&\quad \sum_{n=-\infty}^{\infty} \operatorname{sech}^2\left(\frac{n-\xi}{\lambda}\right) \operatorname{sech}^2\left(\frac{n-\xi}{w}\right) \\
&= \frac{2.75\lambda w}{1.1w+\lambda} - 2\cos(2\pi\xi) \\
&\quad \times \int_{-\infty}^{\infty} \operatorname{sech}^2\frac{x}{\lambda} \operatorname{sech}^2\frac{x}{w} \cos(2\pi x)\,\mathrm{d}x \\
&= \frac{2.75\lambda w}{1.1w+\lambda} - 2I_2(\lambda, w)\cos(2\pi\xi) \\
&\quad \sum_{n=-\infty}^{\infty} \operatorname{sech}^4\left(\frac{n-\xi}{\lambda}\right) \operatorname{sech}^2\left(\frac{n-\xi}{w}\right) \\
&= 1.066 w^{0.2}\lambda^{0.8} + 2\cos(2\pi\xi) \\
&\quad \times \int_{-\infty}^{\infty} \operatorname{sech}^4\frac{x}{\lambda} \operatorname{sech}^2\frac{x}{w} \cos(2\pi x)\,\mathrm{d}x \\
&= 1.066 w^{0.2}\lambda^{0.8} + 2I_3(\lambda, w)\cos(2\pi\xi).
\end{aligned}
$$

The first term in the last two sums is obtained by means of an interpolation of the corresponding integral.

References

[1] Y. Frenkel, T. Kontorova, Zh. Eksp. Teor. Phys. 8 (1938) 89, 1340; J. Phys. 1 (1939) 137.
[2] J.F. Currie, S.E. Trullinger, A.R. Bishop, J.A. Krumhansl, Phys. Rev. B 15 (1977) 5567.
[3] Y. Ishimori, T. Munakata, J. Phys. Soc. Japan 51 (1982) 3367.
[4] M. Peyrard, M. Kruskal, Physica 14D 88 (1984).
[5] R. Boesch, C.R. Willis, M. El-Batanouny, Phys. Rev. B 40 (1989) 2284.
[6] R. Boesch, C.R. Willis, Phys. Rev. B 39 (1989) 361.
[7] P.G. Kevrekidis, M.I. Weinstein, Physica D 142 (2000) 113.
[8] N.F. Smyth, A.L. Worthy, Phys. Rev. E 60 (1999) 2330.
[9] S.P. Novikov, S.V. Manakov, L.P. Pitaevsky, V.E. Zakarov, Theory of Solitons. The Inverse Scattering Transform, Consultants Bureau, New York, 1984.
[10] O.M. Braun, Yu.S. Kivshar, Phys. Rev. B 43 (1991) 1060.
[11] P.G. Kevrekidks, C.K.R.T. Jones, T. Kapitula, Phys. Lett. A 269 (2000) 120–129.